In Situ Infrared Study of 4,4′-Bipyridine Adsorption on Thin Gold Films

Th. Wandlowski,* K. Ataka, and D. Mayer

Institute for Thin Films and Interfaces ISG3, Research Center Jülich, 52425 Jülich, Germany

Received January 28, 2002. In Final Form: March 11, 2002

The phase formation of 4,4′-bipyridine (4,4′-BP) and its coadsorption with interfacial water on quasi-Au(111) film electrodes (20 nm) from 0.05 M $KClO_4$ has been studied employing in-situ surface enhanced infrared reflection adsorption spectroscopy (SEIRAS). Organic molecules form, dependent on the electrode potential and in the absence of Faradaic reactions, three monolayers of distincly different orientation. The high coverage adlayer I is composed of perpendicularly oriented 4,4′-BP molecules coordinated with one nitrogen atom to the underlying positively charged electrodes (C_{2v} symmetry). Changing the electrode potential toward negative values causes two first-order phase transitions giving rise to two low-coverage organic adlayers. These transitions are accompanied by an in-plane tilting of the N-coordinated molecule. The conclusions on the interfacial orientation of 4,4′-BP are supported by a comparative analysis of in situ SEIRAS, surface enhanced Raman spectroscopy, and sum frequency generation spectra. SEIRAS spectra also indicate that 4,4′-BP is coadsorbed with water molecules and modifies the interfacial hydrogen-bonded network of the later. The nature of these interactions and their consequences for the creation of functionalized adlayers on metal electrodes are compared with related N-heterocyclic molecules.

1. Introduction

The electrochemical adsorption of organic molecules is characterized by (1) interactions with the electrode through image charges and/or substrate−adsorbate coordination, (2) displacement of previously adsorbed solvent molecules and/or electrolyte ions, (3) hydrophobic and hydrophilic interactions with remaining solvent molecules, and (4) interactions between the adsorbate species. The latter may involve dispersion and dipole−dipole coupling, π-stacking, and/or hydrogen bonding.[1] Vibrational spectroscopy, such as infrared reflection adsorption spectroscopy (IRAS),[2] sum frequency generation (SFG) spectroscopy,[3] surface-enhanced Raman spectroscopy (SERS),[4] and/or surface-enhanced infrared adsorption spectroscopy (SEIRAS)[5] are powerful techniques for in situ investigations on structure and reactivity aspects of complex interfacial processes under steady-state as well as under dynamic conditions. The combination of SEIRAS and/or SERS with an attenuated total reflection (ATR) configuration provided new insight on the identity and reactivity of interfacial species, such as water, organic molecules, or ions, under potential controlled conditions at defined interfaces.[6−10]

In 1980 Hartstein et al. reported for the first time that the IR absorption of organic molecules, deposited on thin gold and silver films, is remarkably enhanced employing the so-called Kretschmann configuration.[11] Osawa et al. pioneered the application of this technique for equilibrium and time-resolved studies at electrochemical interfaces.[5] The surface-enhanced infrared adsorption effect is attributed to (1) a long-range electromagnetic mechanism (dominant) that involves the excitation of local surface plasmons within thin films of coinage metals and the polarizability perturbation of the metal by the adsorbate species[12] and (2) a short-range chemical contribution similar to the charge-transfer mechanism in SERS.[13,14] The magnitude of the enhanced IR signal, I, depends critically on island structure (size, shape, interparticle spacing, mass thickness) and chemical composition of the metal film.[15] The surface selection rule of SEIRAS states that only molecular vibrations with dipole changes perpendicular to the surface can be observed, which implies that the exciting electric field is normal to the local surfaces of the metal islands at any point and that s-polarized light does not generate any detectable resonance.[5,15] The surface selection rule is represented by the mathematical expression[16]

$$I \sim \Gamma(\mathrm{d}\mu/\mathrm{d}Q)^2 |E^2| \cos^2\theta \sim \Gamma \cos^2\theta$$

where Γ is the surface concentration and θ is the angle between the dipole moment derivative of the vibrational mode $(\mathrm{d}\mu/\mathrm{d}Q)^2$ and the electric filed that excites the molecule $|E^2|$. Consequently, the observed spectral features can be directly ascribed to a specific interfacial orientation of the respective adsorbate. The application of ATR-SEIRAS experiments at solid/liquid interfaces with well-

* To whom correspondence may be addressed: e-mail, th.wandlowski@fz-juelich.de; fax, 49 2461 61 3462; telephone, 49 2461 61 3907.

(1) Guidelli, R. In *Adsorption of Organic Molecules*; Lipkowski, J., Ross, P. N., Eds.; VCH: New York, 1992; p 1.
(2) Iwasita, T.; Nart, F. C. *Prog. Surf. Sci.* **1997**, *55*, 271.
(3) Tadjeddine, A.; Le Rille, A.; Pluchery, O.; Vidal, F.; Zheng, W. Q.; Peremans, A. *Phys. Status Solidi A* **1999**, *175*, 89.
(4) Tian, Z. Q.; Ren, B. In *Encyclopedia of Analytical Chemistry*; Meyers, R. A., Ed.; J. Wiley & Sons: New York, 2001; p 9162.
(5) Osawa, M. *Bull. Chem. Soc. Jpn.* **1997**, *70*, 2861.
(6) Ataka, K.; Osawa, M. *Langmuir* **1998**, *14*, 951.
(7) Watanabe, M.; Zhu, Y.; Uchida, H. *J. Phys. Chem. B* **2000**, *104*, 1762.
(8) Noda, H.; Wan, L. J.; Osawa, M. *Phys. Chem. Chem. Phys.* **2001**, *3*, 3336.
(9) Bruckenbauer, A.; Otto, A. *J. Raman Spectrosc.* **1998**, *29*, 665.
(10) Futamata, M.; Bruckenbauer, A. *Chem. Phys. Lett.* **2001**, *341*, 425.
(11) Hartstein, A.; Kirtley, J. R.; Tsang, J. C. *Phys. Rev. Lett.* **1980**, *45*, 201.
(12) Osawa, M.; Ataka, K.; Yoshi, K.; Nishikawa, Y. *Appl. Spectrosc.* **1993**, *47*, 1497.
(13) Siemes, C.; Bruckbauer, A.; Goussev, A.; Otto, A.; Sinther, M.; Pucci, A. *J. Raman Spectrosc.* **2001**, *32*, 231.
(14) Merklin, G. T.; Griffith, P. R. *Langmuir* **1997**, *13*, 6159.
(15) Suetaka, W. *Surface Infrared and Raman Spectroscopy—Methods and Applications*; Plenum Press: New York, 1995.
(16) Cai, W. B.; Wan, L. J.; Noda, H.; Hibino, Y.; Ataka, K.; Osawa, M. *Langmuir* **1998**, *14*, 6992.

10.1021/la025585k CCC: $22.00
Published on Web 04/26/2002

defined metal films deposited on highly refractive, IR-transparent prisms has several advantages, in comparison to IRAS studies employing the so-called thin electrolyte film configuration (1−5 μm) between the optical window and the working electrode: (1) high and specific surface sensitivity with an enhancement up to ca. 100 times stronger as in conventional IRAS; (2) dominant first layer effect (Helmholtz region) with a short decay length of the enhanced field of 3−4 nm (Gouy region) toward the bulk electrolyte; (3) signals from the interface and the solution background are of comparable magnitude and can be separated by applying the potential difference tactics; (4) no severe limitations due to mass transport and potential perturbations.[5,17]

In this contribution we report an in situ ATR-SEIRAS study in combination with scanning tunneling microscopy (STM) on the phase behavior of 4,4′-bipyridine (4,4′-BP) and water coadsorbed from neutral aqueous solution onto quasi-(111)-oriented thin gold films. The bifunctional nonchelating ligand 4,4′-BP acts as a bridging spacer and coordination unit in 3D and/or 2D supramolecular lattices with novel electric and magnetic properties[18,19,20] and operates as an electron shuttle in the electron transfer of cytochrome *c* on electrochemical interfaces.[21] Michl et al. employed 4,4′-BP with its unique diode-like properties (lone-pair σ-electrons, π,π* orbitals) as a basic building block for "conductive" molecular rods to communicate between functional elements such as "molecular machines" and nanoelectrodes.[19,22] The torsional angle between the two pyridyl rings ranges, depending on environment (soild, liquid, gas phase) and coordination state, between all planar, 18.5° and 37.2°.[23−26] These values reflect the relative contributions of the π-electronic interactions of the pyridyl fragments (favorable to coplanar conformation) and the ortho-bonded interaction of these fragments (favorable to nonplanar structure).

Impedance (capacitance), voltammetric, and electroreflectance experiments indicate a potential-induced reorientation of 4,4′-BP from flat to tilted or perpendicular on mercury,[27] gold,[28−31] silver,[32,33] and platinum electrodes.[34] Wilde et al. speculate, based on EC-quartz crystal microbalance experiments with Au(poly), that 4,4′-BP is coadsorbed with surface water and anions of the supporting electrolyte.[35,36] This idea was supported by a recent in situ ATR study of 4,4′-BP adsorbed under potential control from aqueous sulfuric acid solution onto a thin gold film.[37] Surface coordination of 4,4′-BP in an end-on configuration was suggested from in situ SERS experiments on Au(poly),[38] Ag(poly),[32,33,39−41] and one FTIR study on several metal oxide surfaces.[42] Similar conclusions were also drawn from electron energy loss spectroscopy (EELS) experiments, after transfer of a 4,4′-BP modified Pt(111) electrode into an ultrahigh vacuum (UHV) system.[34] Structural details of the steady state and dynamic phase behavior of up to three ordered 4,4′-BP adlayers on Au(111) were described by Cunha et al.[43] and Mayer et al.[31] in two recent molecular-resolution in situ STM contributions. Umemura[44] and Pinheiro[45] et al. reported results of ex situ investigations on the self-assembly of 4,4′-BP on Au(111) from ethanol solution and its coadsorption behavior with phenanthroline and/or merccaptopyrimidine, respectively.

On the basis of our previous STM work we will present in this contribution a comprehensive in situ ATR-SEIRAS study of the vibrational properties of 4,4′-BP and coadsorbed water species on quasi-single-crystalline Au(111) film electrodes from aqueous electrolytes. The infrared spectra will be compared with SER spectra and results of SFG experiments.

2. Experimental Section

IR Spectroscopy. The SEIRAS experiments were carried out in a vertical spectroelectrochemical cell[46] employing the Kretschmann attenuated total reflection configuration. The working electrode, a thin gold film on a highly resistive (6000 Ω cm) Si hemisphere (25 mm diameter), was prepared by electron beam evaporation at a base pressure of 2×10^{-7} mbar and a deposition rate of (0.005−0.007) nm s^{-1}. The mass thickness, $d_m = 20$ nm, was measured with a quartz crystal microbalance. The corresponding optical thickness, d_o, was estimated by ellipsometry to 23.5 ± 0.5 nm. The gold film consists of preferentially (111) oriented islands with an average diameter ranging between 20 and 30 nm (Figure 1). The metal films were electrochemically annealed by cycling the potential in the double layer region with 50 mV s^{-1}. A typical voltammetric response of the resulting film, as for instance obtained after 30 min in sulfuric acid solution, exhibits well-defined features for the lifting of the ($p \times \sqrt{3}$) reconstruction (P1) and the disorder/order phase transition of an ($\sqrt{3} \times \sqrt{7}$) (hydrogen) sulfate overlayer (P2). These observations are indicative of a high area

(17) Johnson, E.; Avoca, R. *J. Phys. Chem.* **1995**, *99*, 9325.
(18) Steel, P. J. *Coord. Chem. Rev.* **1990**, *106*, 227.
(19) Stoddart, J. F., Ed. *Acc. Chem. Res.* **2001**, *34*, 411 ff.
(20) Chawla, S. K.; Hundal, M. S.; Kaur, J.; Obrai, S. *Polyhedron* **2001**, *20*, 2105.
(21) Armstrong, F. A.; Hill, H. A. O.; Walton, N. J. *Acc. Chem. Res.* **1988**, *21*, 407.
(22) Schwab, R. F.; Levin, M. D.; Michl, J. *Chem. Rev.* **1999**, *99*, 1863.
(23) Boag, N. M.; Coward, K. M.; Jones, A. C.; Pemble, M. E.; Thompson, J. R. *Acta Crystallogr., Sect. C* **1999**, *55*, 672.
(24) Spotswood, T.; Tanzer, C. I. *Aust. J. Chem.* **1967**, *20*, 1227.
(25) Magutova, Y. S.; Maltseva, L. S.; Kamaer, F. G.; Leontev, B. V.; Mikhamedkhanova, S.; Otrosh, O. S.; Sadykev, A. S. *Izv. Akad. Nauk USSR, Ser. Khim.* **1973**, *7*, 1510.
(26) Ould-Moussa, L.; Poizat, O.; Castilla-Ventura, M.; Buntinx, S.; Kassab, E. *J. Phys. Chem.* **1996**, *100*, 2072.
(27) Akhmentov, N. K.; Kaganovich, R. I.; Mambetkaziev, E. A.; Damaskin, B. B. *Electrochimija* **1977**, *13*, 280. Akhmetov, N. K.; Kaganovich, R. I.; Damaskin, B. B.; Mambetkaziev, E. A. *Electrochimija* **1978**, *14*, 176.
(28) Uosaki, K.; Hill, H. O. A. *J. Electroanal. Chem.* **1981**, *122*, 321.
(29) Czerwinski, A.; Zamponi, S.; Sobkowski, J.; Marassi, R. *Electrochim. Acta* **1990**, *35*, 591.
(30) Sagara, T.; Marakami, H.; Igarashi, S.; Sato, H.; Niki, K. *Langmuir* **1991**, *7*, 43.
(31) Mayer, D.; Dretschkow, Th.; Ataka, K.; Wandlowski, Th. *J. Electroanal. Chem.*, in press.
(32) Cotton, M. T.; Varga, M. *Chem. Phys. Lett.* **1984**, *106*, 491.
(33) Liu, T.; Cotton, T. M.; Birke, R. L.; Lombardi, J. R. *Langmuir* **1989**, *5*, 406.
(34) Chaffins, S. A.; Gui, J. Y.; Khan, B. E.; Liu, C. H.; Salaita, G. N.; Stern, D. A.; Zapien, D. C.; Hubbard, A. *Langmuir* **1990**, *6*, 957.
(35) Wilde, C. P.; Ding, T. *J. Electroanal. Chem.* **1992**, *327*, 279.
(36) Zheng, X.; Hatton, R. *Electrochim. Acta* **2000**, *45*, 3629.
(37) Futamata, M. *J. Phys. Chem. B* **2001**, *105*, 6933. Futamata, M. *Chem. Phys. Lett.* **2000**, *332*, 421.
(38) Taniguchi, I.; Iseki, M.; Yamaguchi, H. *J. Electroanal. Chem.* **1985**, *186*, 29.
(39) Wang, X.; Zhao, B.; Wang, Y.; Wu, Y.; Xu, W.; Fan, X. *Mater. Sci. Eng., C* **1999**, *10*, 3.
(40) Miranda, M. *Raman Spectrosc.* **1996**, *27*, 435. Miranda, M.; Neto, N.; Sbrana, G. *J. Mol. Struct.* **1997**, *410−411*, 205.
(41) Rubim, J. C.; Temperini, M. L. A.; Corio, P.; Sala, O.; Hubert, A. H.; Chacon-Villalha, M. E.; Aymonino, P. J. *J. Phys. Chem.* **1995**, *99*, 345.
(42) Bagshaw, S. A.; Cooney, R. P. *Appl. Spectrosc.* **1996**, *50*, 310.
(43) Cunha, F.; Tao, N. J.; Wang, X. W.; Jin, Q.; Duong, B.; DeAgnese, J.; *Langmuir* **1996**, *12*, 6410.
(44) Umemura, K.; Nishida, N.; Hara, M.; Sasabe, H.; Knoll, W. *J. Electroanal. Chem.* **1997**, *438*, 207.
(45) Pineirho, L. S.; Temperini, M. L. A. *Appl. Surf. Sci.* **2001**, *171*, 89.
(46) For details see: Wandlowski, Th.; Diesing, D.; Ataka, K. *Phys. Chem. Chem. Phys.*, in preparation.

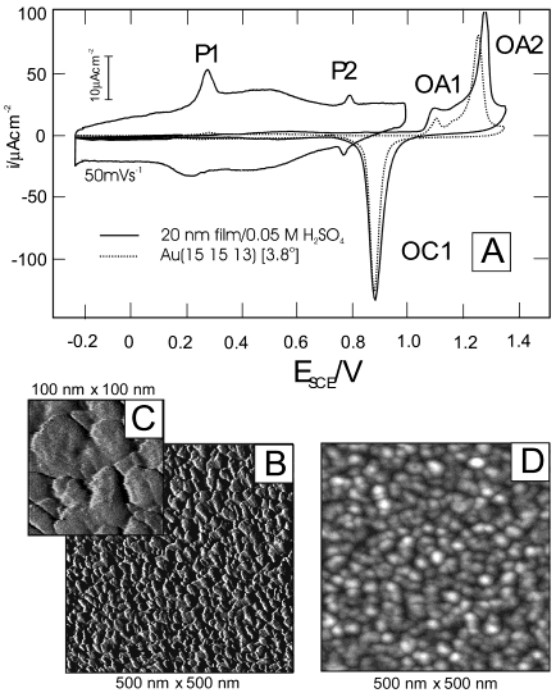

Figure 1. (A) Cyclic voltammograms of quasi-(111) Au (20 nm) film (solid lines) and stepped Au(15 15 13) (dotted lines) electrodes in contact with 0.05 M H_2SO_4, scan rate 10 mV s^{-1}. The curve showing just the double layer region was recorded with 50 mV s^{-1} and is plotted in a magnified current scale as indicated. Panels B, C, and D show ex situ STM and AFM images of the Au (20 nm) film electrodes, as obtained immedeately after evaporation.

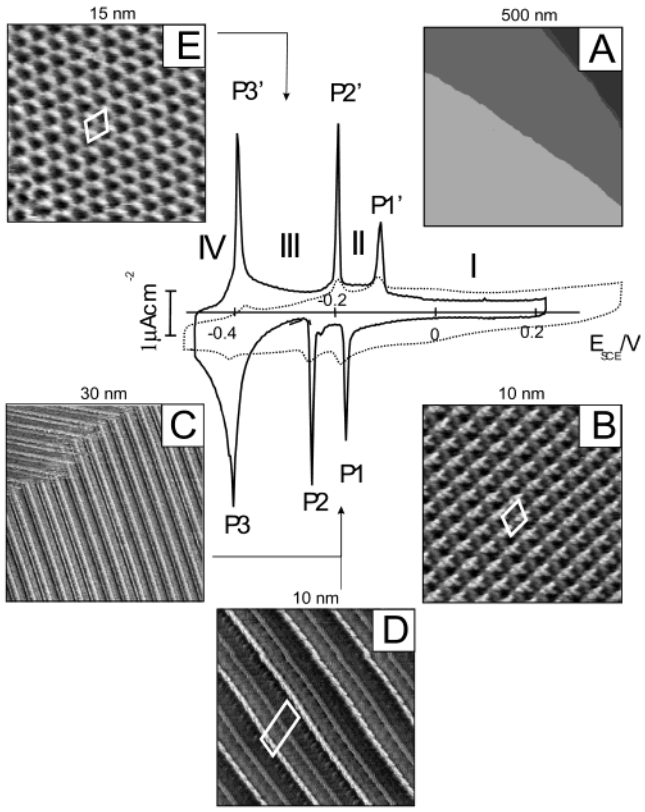

Figure 2. Cyclic voltammogram for Au(111) (solid line) or Au (20 nm (111)) (dotted line)/0.05 M $KClO_4$ in the presence of 3 mM 4,4′-BP, scan rate 10 mV s^{-1}. In situ STM images represent various stages of the potential-dependent adsorption/phase formation processes: (A) electrochemically annealed Au(111)−(1 × 1) surface at 0.20 V; (B) 4,4′-BP adlayer I at 0.17 V; (C, D) 4,4′-BP adlayer II at −0.23 and at −0.21 V; (E) organic adlayer at −0.32 V. The corresponding unit cells are indicated. The stability regions of the various adlayer phases are labeled I−IV.

percentage of (111)-oriented terrace sites.[47] The direct comparison of the oxidation/reduction fingerprint region with current vs potential curves measured with stepped single crystals, Au[n(111) × (110)], yields a rather comparable response of our film with Au[15(111) × (110)] (miscut angle of 3.8° with respect to an ideal (111)-terminated surface), assuming a roughness factor of 2 (Figure 1).

The infrared spectra were measured with a Bruker IFS 66V/s, choosing a spectral resolution of 4 cm^{-1}. Unpolarized infrared radiation from a globar source was focused onto the electrode/electrolyte interface by passing through the silicon prism (cf. surface selection rules and ref 46). The incident angle was 70° referred to the surface normal. The radiation totally reflected at the interface was measured with a liquid nitrogen cooled MCT detector (MCT 316, Colmar Technologies). Typically, 200 interferograms were scanned and coadded into each single-beam spectrum (200 kHz scanning rate of the interferometer). The spectra were plotted in absorbance units defined as $A = -\log(I/I_0)$, where I and I_0 represent the intensities of the reflected radiation at sample and reference potentials, respectively. The acquisition of spectra was performed either at constant potential or during a slow potential sweep with 5 mV s^{-1}. The electrode potential was controlled and synchronized with a HEKA potentiostat PG 310.

Scanning Tunneling Microscopy. The STM and atomic force microscopy (AFM) experiments were carried out with a Molecular Imaging Pico-SPM. The STM tips were electrochemically etched Pt/Ir tips (70/30, 0.25 mm diameter), coated with polyethylene. The in situ experiments were performed with a platinum wire and a gold oxide microelectrode as counter and reference electrodes, respectively. All STM images were recorded at room temperature in constant current mode with tunneling currents ranging between 3 and 200 pA.

Single-Crystal Electrodes and Solutions. The smooth Au(111) or stepped Au(n n n − 2) = Au[n(111)−(110)] electrodes were either single-crystal cylinders (4 mm diameter, 4 mm height, EC) or disks (10 mm diameter and 2 mm height, STM). Before each measurement the massive gold single crystals were flame annealed in a butane flame at red heat and then cooled in high-purity argon. Contact with the electrolyte was established under potential control. All potentials in this paper are quoted with respect to the saturated calomel electrode (SCE).

The solutions were prepared with Milli-Q water (18 MΩ cm, 3 ppb TOC), H_2SO_4 (suprapure, Merck), $KClO_4$ (Fluka, puriss p.a., twice recrystallized from water). All electrolytes (EC, SEIRAS) were deareated with argon prior to and during each experiment. The measurements were carried out at 20 ± 0.5 °C.

Details of the SERS and SFG will be reported elsewhere.[48,49]

3. Results and Discussion

3.1. Electrochemistry and Scanning Tunneling Microscopy. Figure 2 shows typical cyclic voltammo-

(47) Dretschkow, Th.; Wandlowski, Th. *Ber. Bunsen-Ges. Phys. Chem.* **1997**, *101*, 749.

(48) Wandlowski, Th.; Lin, W. T.; Huong, Z.; Ren, F. R.; Tian, Z. Q. *Chem. Phys. Lett.*, in preparation.

(49) Wandlowski, Th.; Busson, B.; Vidal, F.; Tadjeddine, A., in preparation.

grams of 3 mM 4,4′-BP adsorbed from aqueous 0.05 M $KClO_4$ solution (pH ~ 5.8) onto a perfect Au(111)−(1 × 1) single-crystal electrode (solid line, Figure 2) or onto a quasi (111) single crystalline 20 nm thick Au film (dotted line). The latter is supported on a silicon prism. 4,4′-BP molecules assume under these conditions in the bulk electrolyte their unprotonated form ($pK_{a1} = 3.5$; $pK_{a2} = 4.9$[50]). Both sets of data indicate clearly the existence of four different potential regions labeled I−IV, which are separated by distinct charging current peaks P1/P1′, P2/P2′, and P3/P3′. Remarkable is the large hysteresis between the positive and negative potential scans. The experiments with the massive single crystal exhibits non-Faradaic phase transitions, which are higher and narrower in comparison with those of the film electrodes. The center peak positions obtained with both types of electrodes are rather similar. These observations correlate with the smaller terrace size and higher defect density of the latter (cf. Figure 1). Similar trends were also reported for order/disorder phase transitions in (hydrogen) sulfate adlayers[47] and physisorbed uracil films on stepped gold electrodes.[51]

The stability of range I is delimited at positive potentials by the competing adsorption of OH^-, and the onset of gold oxidation,[52] and at negative potentials by the current peaks P1/P1′. Steady-state in situ STM images of adlayer I revealed a periodic array of bright features with characteristic unit cell dimensions of $a = 1.10$ nm ($\approx 4a_{Au}$), $b = 1.25$ nm, and $\alpha = 76.5°$ (Figure 2B). This result, the analysis of high-resolution contrast patterns and domain properties, as well as packing considerations, motivated the hypothetical interpretation of I as a densely packed monolayer of interdigitated, perpendicularly oriented 4,4′-BP molecules (six molecules per unit cell, surface concentration $\Gamma_{mI} = 6.9 \times 10^{-10}$ molecules cm^{-2}), which are stabilized by N-coordination with the positively charged electrode surface and lateral π stacking.[31,43] The high-density phase transforms upon negative potential excursion into a new striped pattern II (Figure 2C) according to a progressive hole nucleation process combined with surface diffusion-controlled growth.[31] High-resolution STM images, such as Figure 2D, revealed additional structural details. Assigning tentatively each "elongated" blob to an N-coordinated 4,4′-BP molecule, one may imagine a pattern of four parallel stacking rows. We proposed recently a high-order commensurate phase with $a = 1.15$ nm ($=4a_{Au}$), $b = 2.5$ nm, and $\alpha = 74°$, which contains nine molecules.[31] The corresponding area per molecule and coverage were estimated as $A_{II} = 0.29$ nm^2 and $\Gamma_{mII} = 5.7 \times 10^{-10}$ molecules cm^{-2}.

4,4′-BP molecules assemble into a third ordered adlayer just after crossing the current peak P2 toward negative potentials. STM experiments at rather low tunneling currents yield a regular rhombohedral arrangement of dark (or bright) spots (Figure 2E), which could be resolved at higher tunneling voltages into individual 4,4′-BP molecules arranged in parallel stacking rows.[31] The suggested unit cell with $a = 1.15$ nm, $b = 1.3$ nm, and $\alpha = 71°$contains three molecules with $A_{III} = 0.47$ nm^2 and $\Gamma_{mIII} = 3.4 \times 10^{-10}$ mol cm^{-2}.

The reduction of 4,4′-BP into its anion radical takes place at potentials more negative than P3/P3′.[31,38] Capacitance experiments indicate incomplete desorption. Returning the negative-going potential scan before the onset of 4,4′-BP reduction yields in -0.500 V $< E <$ 0.250 V the quasi-steady-state voltammetric response as plotted in Figure 2. The three differently ordered organic adlayers can be repeatedly created and dissolved during multiple potential cycles.

The electrochemical and STM experiments indicate that the transition between the high coverage 4,4′-BP adlayer I toward the phases II and III might be tentatively represented by the successive loss of parallel stacking rows, reducing the coverage from 6.8×10^{-10} mol cm^{-2} via 5.7×10^{-10} mol cm^{-2} to 3.4×10^{-10} mol cm^{-2}. Unfortunately, the strong variation of the STM contrast pattern of the present system with the applied tunneling conditions, especially the tunneling current, i_T, and the tunneling voltage, V_T, as discussed in ref 31, do not provide an unambiguous understanding of the potential-dependent interfacial orientations of 4,4′-BP and their interaction with solvent (water) molecules and/or ions of the supporting electrolyte. These aspects shall be addressed in the following in situ SEIRAS study.

3.2. Vibrational Spectroscopy, SEIRAS. 3.2.1. Absolute Spectra at Constant Potential and Kinetics of Adlayer Formation. The SEIRAS experiment started with a freshly deposited 20 nm thick gold film as working electrode in contact with 0.1 M aqueous $KClO_4$ solution. After the electrolyte was deoxygenated, the films were electrochemically annealed by cycling the electrode potential with 50 mV s^{-1} in the double layer region (-0.60 V $< E <$ 0.60 V) until a steady-state response of the electrochemical and spectroscopic signals was obtained (cf. refs 53 and 54).

Due to the incomplete desorption of 4,4′-BP and the onset of reduction to form the anion radical at negative potentials, absolute absorbance spectra were measured first in the stability range of phase I at constant potential ($E = 0.200$ V). The adsorbate-free 0.1 M $KClO_4$ solution served as in situ reference. After addition of 3 mM 4,4′-BP into the stirred electrolyte (argon bubbling) single-beam spectra, obtained from the average of 200 coadded interferograms, were acquired every minute. Positive-going bands indicate accumulation of the species with respect to the reference, which is represented by the 4,4′-BP-free electrolyte. Typical SEIRA spectra of such an experiment are plotted in Figure 3. A steady-state spectral response is obtained after approximately 20 min. The most prominent positive-going broad bands in the region 3200 $cm^{-1} < \nu < 3700$ cm^{-1} and around 1656 ± 3 cm^{-1} (fwhm = 87 cm^{-1}) are assigned to OH stretching (ν_{OH}) and HOH bending (δ_{HOH}) modes of coadsorbed water species.[53] The positive sign indicates that the intensity increases with respect to the reference spectrum, e.g., the adsorption of 4,4′-BP increases the amount of oriented, coadsorbed water molecules within the double layer region and/or facilitates the formation of strongly hydrogen-bonded interfacial water (Helmholtz, Gouy region).[55] With the assumption of Gaussian band shapes, the OH stretching modes could be deconvoluted into three contributions, centered at 3605 ± 3 cm^{-1} (fwhm 99 ± 4 cm^{-1}), 3484 ± 2 cm^{-1} (fwhm 214 ± 4 cm^{-1}), and 3308 ± 2 cm^{-1} (fwhm 390 ± 8 cm^{-1}), respectively. As a typical example, a set of fitting curves is plotted in Figure 3A. The narrow band around 3605 cm^{-1} indicates the presence of non-hydrogen bonded OH,[55] while the broad ν_{OH} bands at 3484 and 3308 cm^{-1} are assigned to strongly hydrogen-bonded OH and a Fermi resonance between ν_{OH} and the binary overtone of δ_{HOH}.[53]

(50) *Encyclopedia for Chemistry, Basic Part II*, 4th ed.; Chemical Society of Japan: Tokyo, 1993; Chapter 10.
(51) Bare, S.; van Krieken, M.; Buess-Herman, C.; Hamelin, A. *J. Electroanal. Chem*. **1998**, *445*, 7.
(52) Angerstein-Kozlowska, H.; Conway, B. E.; Hamelin, A.; Stoicoviciu, N.; *J. Electroanal. Chem*. **1987**, *228*, 429.
(53) Ataka, K.; Yotsuyangi, T.; Osawa, M. *J. Phys. Chem*. **1996**, *100*, 10664.
(54) Ataka, K.; Osawa, M. *J. Electroanal. Chem*. **1999**, *460*, 188.
(55) Thiel, P. A.; Madey, T. E. *Surf. Sci. Rep.* **1987**, *7*, 211.

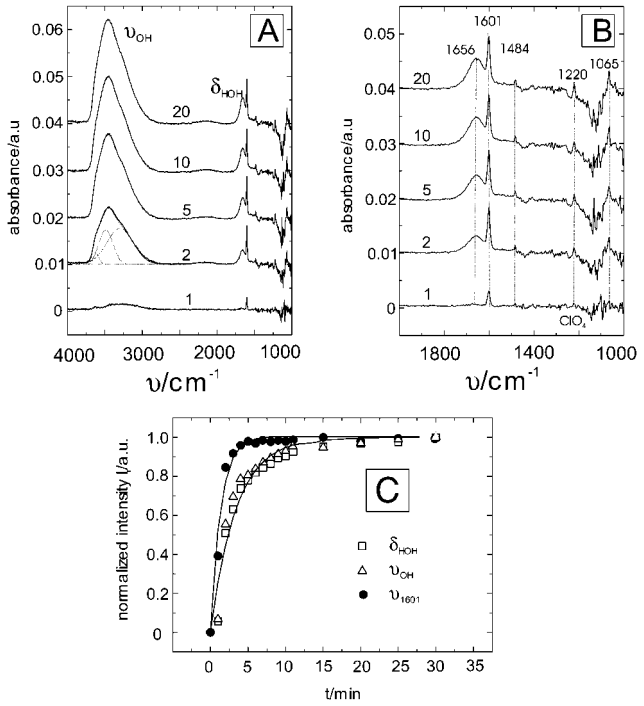

Figure 3. Series of "absolute" SEIRAS spectra of a highly ordered Au(111) surface in 0.05 M $KClO_4$ as a function of time (indicated in minutes in (A) and (B)) after addition of 3 mM 4,4′-BP at $E = 0.20$ V. The reference spectrum was measured at $t = 0$ min in the absence of the organic molecule. A typical example of the deconvolution of the OH-stretching region into three Gaussian contributions is also indicated in panel (A). (C) Time dependence of the normalized intensities of δ_{HOH}, ν_{OH}, and ν_{1601} (4,4′-BP). The solid lines represent fits to eq 1.

The band center positions and ratios of the integrated intensities of these three contributions do not significantly change with the accumulation time of 4,4′-BP. The later was estimated as 5:33:62. Comparison with the corresponding spectral response of the adsorbate-free electrolyte[53] indicates that 4,4′-BP modifies the network of hydrogen-bonded interfacial water species. Referring to the previously reported ability of heterocyclic molecules such as cytosine,[54] pyridine,[56] 2,2′-bipyridine,[57] or pyrazine[58] to replace interfacial water, the present result is rather different and points to a strong hydrophilic character of 4,4′-BP adsorption on Au(111). The spectral features of water at the interface are also different from the spectrum of the bulk electrolyte, which implies that the background absorption of the bulk solution is completely subtracted.

Expansion of the spectrum into the "fingerprint" region between 1000 and 2000 cm^{-1} revealed the bands (Figure 3B), characteristic of adsorbed 4,4′-BP, at 1065 (w), 1220 (w), 1484 (w), and 1601 cm^{-1} (s), which increase in intensity with increasing interfacial coverage of 4,4′-BP. No peak shifts were observed, suggesting that molecule−molecule and molecule−substrate interactions are constant during the adsorption process. These four bands were found at rather similar frequencies in the KBr spectrum of the molecule and are attributed to a ring in-plane deformation + ring stretching (ν_{18a}), CH in-plane bending (ν_{9a}), CH in-plane bending + ring stretching (ν_{19a}), and a prominent

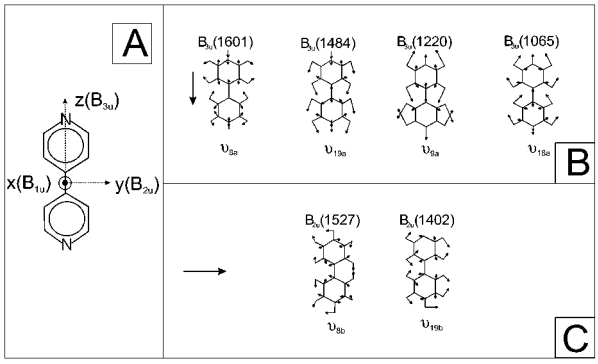

Figure 4. Molecular coordinate system (A) and normal modes of experimentally observed in-plane B_{3u} and B_{2u} vibrations, with the spectral assignment taken from refs 26, 59, and 60.

ring stretching mode (ν_{8a}).[26,59,60] The corresponding Wilson notation is given in parantheses. Referring to the D_{2h} symmetry of the "free" 4,4′-BP molecules all vibrations observed in the potential region of the adlayer I in 1000 $cm^{-1} < \nu < 4000$ cm^{-1} represent in-plane B_{3u} modes; no B_{2u} modes were observed (Figure 4). The negative-going (loss) band around 1130 cm^{-1} is attributed to the replacement of interfacial ClO_4^- ions.[53] The spectral range below 1000 cm^{-1} could not be analyzed due to the strong absorption of the silicon prism.

Finally we note that similar observations were made at any other potentials within the stability range of region I.

The time dependence of the normalized (with the corresponding steady-state response at $t = 30$ min, $E = 0.200$ V, as reference), integrated intensities of ν_{1601}, the most intense vibrational mode of adsorbed 4,4′-BP, and the two water features, ν_{OH} and δ_{HOH}, is plotted in Figure 3C. ν_{1601}, as a typical representative of the observed B_{3u} modes of 4,4′-BP reaches saturation after 5 min, while the establishment of the steady-state response of both interfacial water modes, which exhibit rather identical time dependencies, requires approximately 20 min. These spectroscopically obtained correlations between relative intensity I_r and time t can be represented by a first-order kinetic equation

$$I_r = 1 - \exp(-kt) \qquad (1)$$

with k as an apparent rate constant. Curve fitting of eq 1 to the experimental transients (solid line in Figure 3C) yields $k(\nu_{1601}) = 0.73 \pm 0.03$ min^{-1}, and $k(\nu_{OH}, \delta_{HOH}) = 0.30 \pm 0.02$ min^{-1}.

These results indicate that the formation of the high coverage 4,4′-BP adlayer (with reference to the adsorbate free base electrolyte, cf. ref 31) is accompanied by major, and obviously even slower ordering of interfacial water molecules within the Helmholtz and Gouy regions, both of which are probed. The penetration depth of SEIRA in our configuration does not access further contributions from the bulk electrolyte.[5]

3.2.2. Potential Dependence of 4,4′-BP Adsorption on Au(20 nm-111). After a steady-state spectral response was reached in region I at 0.200 V, the potential was slowly scanned with 5 mV s^{-1} toward −0.500 V (limit of the non-Faraday adsorption range of 4,4′-BP[31,43]) and then back to 0.200 V. The "relative" in situ SEIRA spectra were recorded simultaneously, choosing the steady-state single-beam spectrum of the high coverage 4,4′-BP phase I at

(56) Cai, W. B.; Wan, L. J.; Noda, H.; Hibino, Y.; Ataka, K.; Osawa, M. *Langmuir* **1998**, *14*, 6992.
(57) Noda, H.; Minoka, T.; Wan, L. J.; Osawa, M. *J. Electroanal. Chem.* **2000**, *481*, 62.
(58) Cai, W. B.; Amanov, T.; Osawa, M. *J. Electroanal. Chem.* **2001**, *500*, 147.
(59) Kihara, H.; Gondo, Y. *J. Raman Spectrosc.* **1986**, *17*, 263.
(60) Topacli, A.; Akyuz, S. *Spectrochim. Acta, A* **1995**, *51*, 633.

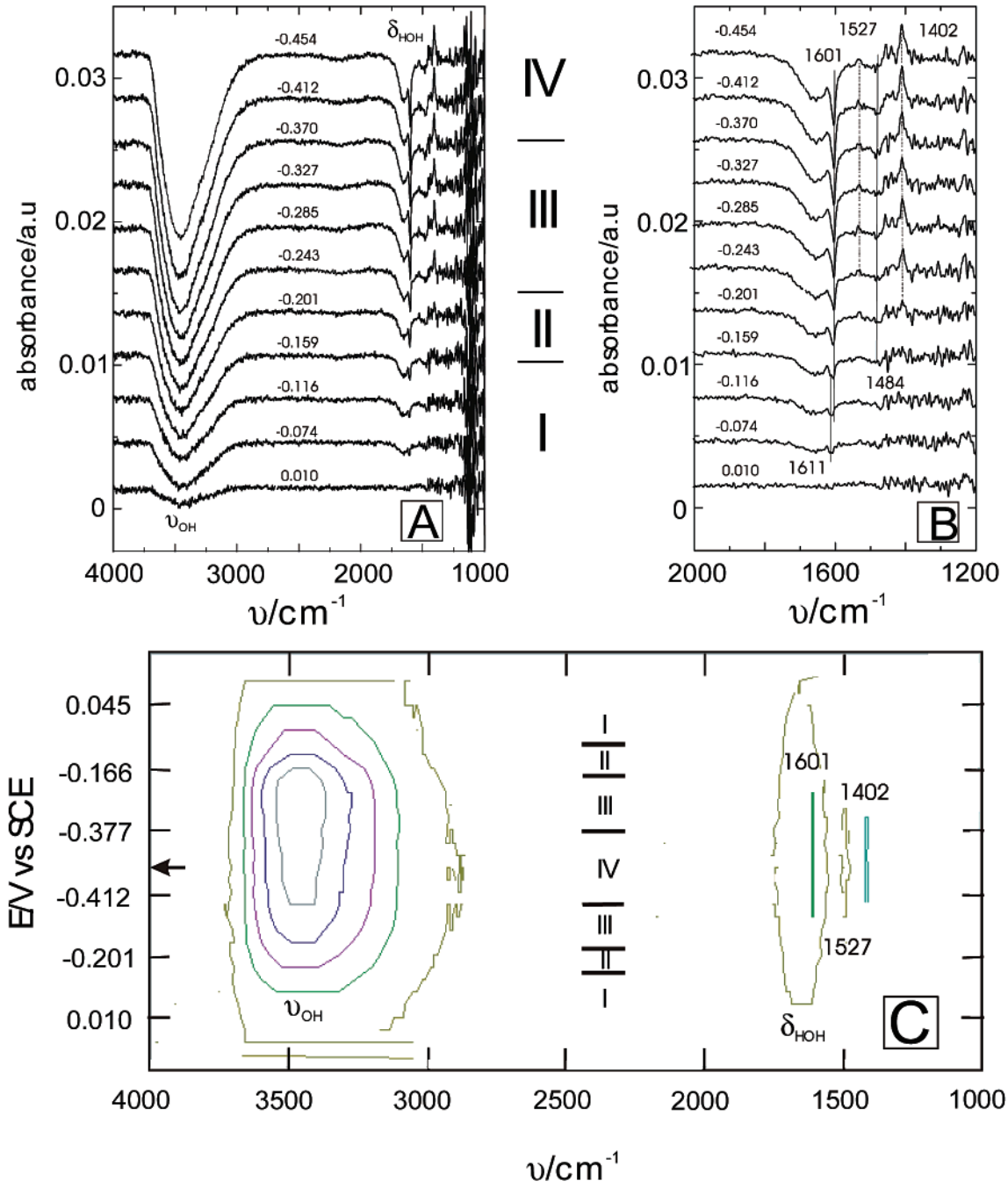

Figure 5. Selected SEIRAS spectra of 3 mM 4,4′-BP adsorbed on an Au (20 nm (111)) electrode in 0.05 M $KClO_4$ as a function of potential, measured simultaneously with a slow scan voltammogram (5 mV s^{-1}, negative potential sweep): (A) overview spectra; (B) zoom-out of the low-frequency range; (C) contour plot. 200 single scans are averaged within each potential interval of 42 mV. The reference spectrum was measured at 0.20 V (phase I).

0.200 V as reference. The IR spectra were acquired sequentially at every 42 mV, by averaging of 200 individual interferograms. Parts A and B of Figure 5 illustrate typical sets of selected relative spectra as obtained during a sweep toward negative potentials. (We note that downward bands represent loss features with respect to the reference state.[5]) The contour plot in Figure 5C represents the spectral response of one complete voltammetric cycle. Clearly developed and monotonically growing loss features of interfacial water occur in the OH-stretching (3200 $cm^{-1} < \upsilon < 3700\ cm^{-1}$) and the HOH-bending (1656 cm^{-1} shifts toward 1646 cm^{-1}) regions as well as for the B_{3u} modes of 4,4′-BP around 1601 (s) and 1484 cm^{-1} (w) with increasing negative potentials (Figure 5). The potential-dependent integral loss intensities of υ_{OH}, υ_{HOH}, and υ_{1601} are plotted in Figure 6A.

Careful inspection of the potential evolution of the prominent stretching mode reveals that upon approaching the voltammetrically determined transition potential P1, an initially splitted double band with centered positions at 1611 and 1601 cm^{-1} develops. After passing P1, only the loss feature around 1601 cm^{-1} increases further in regions II, III, and IV (Figure 5B). A similar splitting of other B_{3u} loss bands could not be detected because of the rather poor signal-to-noise ratio for υ_{1484} and the other two B_{3u} bands below 1250 cm^{-1}. Nevertheless, this observation may indicate site-specific desorption and/or structural changes within the high coverage 4,4′-BP phase.

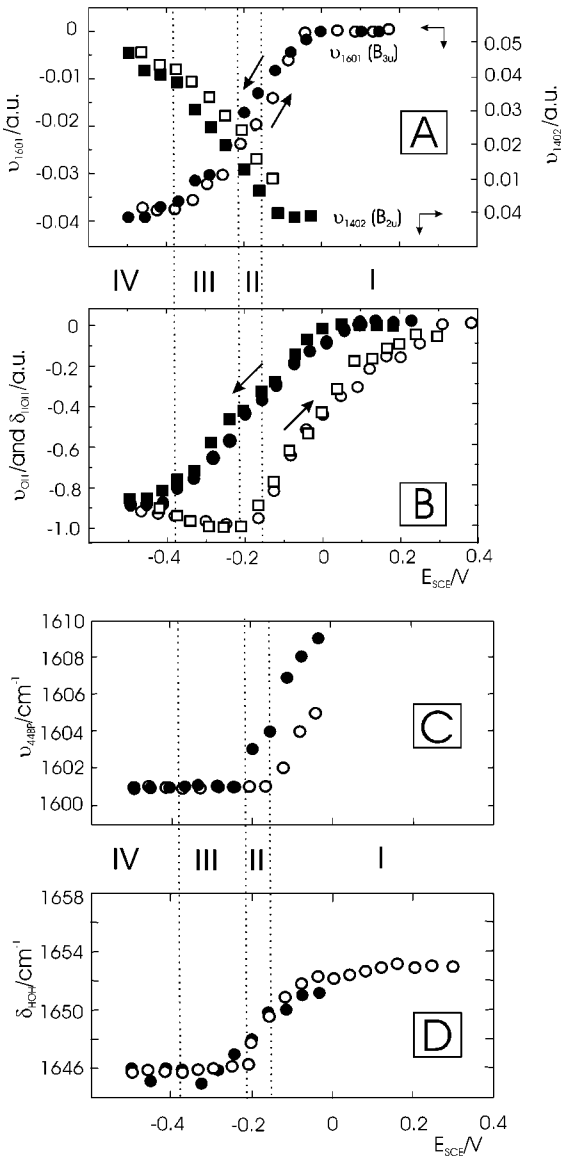

Figure 6. Potential dependence (A) of the integrated intensities of the ν_{1601} (B_{3u}; ○, ●) and ν_{1402} (B_{2u}; □, ■) and (B) of the normalized interfacial water vibrations ν_{OH} (○, ●), δ_{HOH} (□, ■). (C), (D) potential dependence of the band positions of ν_{44BP} and δ_{HOH}. The open (filled) symbols represent data aquired during a positive (negative) potential scan.

Similar arguments were recently discussed for pyridine. Hoon-Koshla et al. pointed out that the in-plane ring deformation mode of N-bonded pyridine on Au(111) splits into a small band at ~1599 cm^{-1} associated to defect sites, and a main band at 1593 cm^{-1} (lower wavenumbers!) representing pyridine on (111) terraces.[61]

Simultaneously and correlated to the loss features of interfacial water and of B_{3u} 4,4′-BP modes, two new bands start to grow (positive!) at $\upsilon \sim 1402$ cm^{-1}, and a weaker feature at 1527 cm^{-1} (Figure 5). Both could be assigned to in-plane B_{2u} modes of adsorbed 4,4′-BP, specifically to the in-plane bending + ring stretching mode (υ_{19b}, ~1402 cm^{-1}) and the ring stretching mode (υ_{8b}, ~1527 cm^{-1}).[26,59,60] The peak positions are independent of the electrode potential.

These structural changes of adsorbed 4,4′-BP and coadsorbed water are reproducible during multiple cycling. Changing the direction of the slow potential scan (negative as illustrated in Figure 5, positive not shown) causes a significant hysteresis in the evolution of the respective vibrational modes. Figure 6 illustrates, as a summary of these observations, the potential dependence of the integrated intensities of the two most intense modes of adsorbed 4,4′-BP, υ_{1601} (B_{3u}), υ_{1402} (B_{2u}), and of interfacial water, υ_{OH} and δ_{HOH}. The position of the B_{3u} mode does not change with potential in -0.600 V $< E < -0.500$ V, except of the already described satellite feature at 1611 cm^{-1} around P1. During the negative-going potential scan, the integrated intensity of the ν_{1601} loss band (B_{3u}) decreases initially rather moderately (still in region I), followed by a steep decrease at $E < -0.100$ V (voltammetric peak P1, I → II), which slows somewhat down at $E < -0.250$ V (II → III) until it levels off at $E < -0.400$ V (P3, region IV). The subsequent positive-going scan is represented by an initial small slope, which increases in two slightly separate steps at $E > -0.400$ V (P3′, IV → III) and at $E > -0.220$ V (~P2′, III → II) until the slope levels off at $E > 0.050$ V (~P1′, II → I). The hysteresis of approximately 50 mV between the forward and backward potential scans and the changes in slope of the loss-intensity vs potential plots correlate nicely with peak position and hysteresis of the corresponding voltammetric response (Figure 2). Similar correlations were found for the ν_{1402} gain mode (B_{2u}). The negative potential scan exhibits a steep increase of the integrated intensity in region II ($E < -0.100$ V, I → II), a moderate change in region III until the change levels off in region IV at $E < -0.400$ V (III → IV). The potential dependencies of the integrated intensities of ν_{OH} and δ_{HOH} are identical (normalized representation in Figure 6B) and reflect changes in the four stability regions of adsorbed 4,4′-BP, and around the various phase transitions, but do not strictly correlate with the exact positions predicted from the voltammetric experiments. Remarkable is the hysteresis of approximately 0.200 V between the responses of the negative and positive potential scans (e.g., four times that of the 4,4′-BP modes). The water relaxation appears to be more pronounced within the IR-probed interfacial region than the sole rearrangement of the 4,4′-BP molecules. Interestingly, the latter seems to dominate the charging current−potential or time response (voltammetry, chronoamperometry). Deconvolution of the complex ν_{OH} stretching mode, with the assumption of Gaussian line shapes, reveals three components centered at 3600 ± 7 (fwhm ~ 110 ± 10 cm^{-1}), 3484 ± 5 (fwhm ~ 210 ± 7 cm^{-1}), and 3315 ± 20 cm^{-1} (fwhm ~ 330−370 cm^{-1}), rather independent of the applied electrode potential, and with relative contributions of 5:35:60. These results are similar to those reported previously for the absolute spectra in region I. The center position of the δ_{HOH} bending mode shifts with potential from 1654 ± 1 cm^{-1} in region I ($E > -0.100$ V) to lower wavenumbers, 1646 ± 2 cm^{-1} in region IV (Figure 6D). This trend indicates a slight but significant decrease of interfacial hydrogen bonding. Compared with the perchlorate containing electrolyte in the absence of 4,4′-BP, the position of the δ_{HOH} mode occurs at negative potentials at higher wavenumbers (1646 cm^{-1} instead of 1612 cm^{-1} [53]), which clearly represents the promotion of hydrogen bonding in the presence of 4,4′-BP.

No change of the baseline or background reflectivity of the electrode was observed within the potential range of an ideal polarizable Au(20 nm)/0.1 M $KClO_4$ + 3 mM 4,4′-BP interface. The reflectance change in the IR region represents predominantly the optical properties of the metal substrate. In consequence, one may conclude that

(61) Hoon-Koshla, M.; Fawcett, W. R.; Cheng, A.; Lipkowski, J.; Pettinger, B. *Electrochim. Acta* **1999**, *45*, 611.

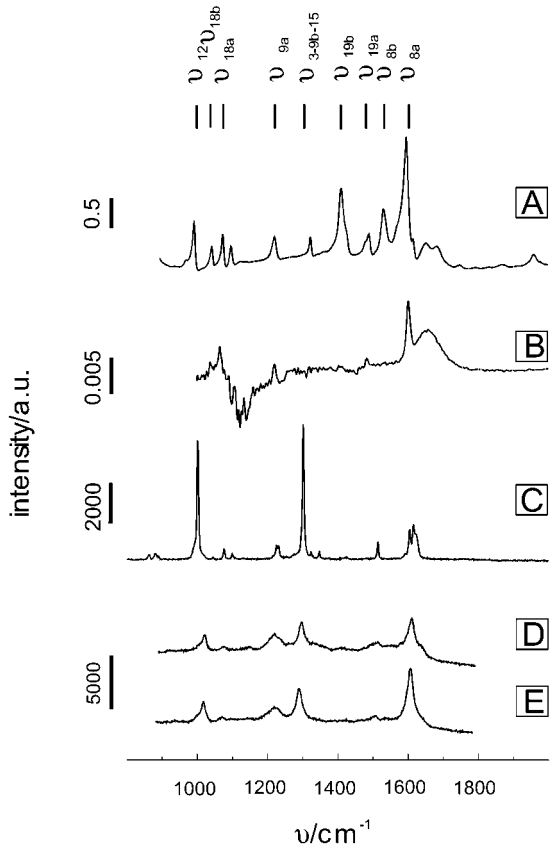

Figure 7. Comparison of IR and Raman spectra of 4,4′-BP: (A) IR spectrum of crystalline 4,4′-BP; (B) SEIRAS spectrum of 3 mM 4,4′-BP in 0.05 M $KClO_4$/Au (20 nm (111)) at 0.20 V; (C) Raman spectrum of crystalline 4,4′-BP ($\lambda = 632$ nm); (D, E) SERS spectra of 3 mM 4,4′-BP in 0.05 M $KClO_4$ on a roughened Au(poly) electrode[48] at 0.20 and −0.60 V.

4,4′-BP interacts weakly with Au(20 nm) and does not change its optical properties upon adsorption.

4. Discussion

4.1. Molecular Orientation of 4,4′-BP in Region I. The free 4,4-BP molecule (crystalline, solution vapor phase) exhibits D_{2h} symmetry with 54 fundamental vibrational modes. The IR ($5B_{1u}$, $9B_{2u}$, $9B_{3u}$) and Raman modes ($10A_g$, $9B_{1g}$, $5B_{2g}$, $3B_{3g}$), cf. definition of *xyz* molecular axes as shown in Figure 4, are mutually exclusive. The four remaining A_u modes are neither IR nor Raman active. The two pyridine rings contribute equally to the electronic and hence vibrational properties of the molecule. This situation changes if 4,4′-BP adsorbs on a metal surface[31−33,37−39,41] and/or coordinates with metal ions.[60] Monodentate substrate−adsorbate coordination via the nitrogen atom of one of the pyridine rings reduces the symmetry of the adsorbed 4,4′-BP from D_{2h} to C_{2v}, which predicts identical IR and Raman modes (cf. pyridine,[56,61] 2,2′-BP,[57] or pyrazine[58]). The D_{2h} and C_{2v} fundamentals, referred to the coordinate system in Figure 4, are related as follows: $B_{3u} + A_g \rightarrow A_1$; $B_{2u} + B_{1g} \rightarrow B_2$; $B_{1u} + B_{2g} \rightarrow B_1$; $A_u + B_{3g} \rightarrow A_2$.

The SEIRAS spectra in region I ($E > -0.100$ V) exhibit four bands of adsorbed 4,4′-BP (ν_{1065} (ν_{18a}) (w), ν_{1220} (υ_{9a}) (w), υ_{1484} (ν_{19a}) (w), υ_{1601} (ν_{8a}) (s); Figure 3B, Figure 7B), which could be assigned to in-plane B_{3u} modes. They represent changes of the molecular dipole moment along the *z* axis (Figure 4). None of the B_{2u} vibrations (dipole changes along the in-plane *y* axis), rather strong in the crystalline phase or in solution (υ_{1411} (ν_{19b}), υ_{1532} (ν_{8b} = 1532);[60] Table 1, Figure 7A), was observed. In addition, the position of the ring stretching mode $\nu_{8b} = 1601$ cm^{-1} (B_{3u}), which is sensitive to the interaction of the pyridine nitrogen with electron acceptors,[60,62] shifts, in comparison to the response of the pure solid sample, toward slightly higher wavenumbers (Table 1) indicating substrate adsorbate coordination.[63] On the other hand, the small peak shift and the potential-independent background intensity suggest a rather weak interaction between 4,4′-BP and the positively charged gold surface. By application of the surface selection rule in SEIRAS that only normal components of the dipole change are IR active (cf. Introduction and refs 5 and 15), the preferential observation of B_{3u} modes in region I is interpreted such that 4,4′-BP is adsorbed via one nitrogen atom in an end-on configuration with the C_2 rotation axis of the molecule being perpendicular to the surface or with the *y* axis parallel to the surface. No IR-forbidden modes, as for instance discussed in the case of pyrazine on rough gold surfaces, were found.[58,64] Flat-lying and edge-on configurations are clearly discarded. The frequency region below 1000 cm^{-1}, where out-of-plane modes occur, was not accessible in our IR experiments due to the cutoff of the silicon prism. Nevertheless, the tilted orientation can be excluded, based on in situ SERS experiments with polished[48] or roughened (oxidation/reduction cycles)[38] polycrystalline gold electrodes (Figure 7D,E). No out-of-plane Raman modes, B_{2g}, were found. The SER spectrum in region I is dominated by the symmetrical vibrational modes A_g (Figure 7D,E), which correspond to a perpendicular end-on orientation of 4,4′-BP and strengthen the molecular packing model suggested from the STM experiments[31] (Figure 9). These spectral features are similar to those observed on silver electrodes.[32,33] Except for the interring stretching mode υ_{1289} (Ω) and for the ring mode ν_{1021}

Table 1. Characteristic Vibrational Modes of 4,4′-BP[a]

A. IR (crystal), in Situ SEIRAS, and SFG Experiments

mode (symmetry)	IR υ/cm^{-1} bulk crystal	SEIRAS υ/cm^{-1} Au (20 nm) film	SFG υ/cm^{-1} Au(111)
υ_{12} (B_{3u})	992		
υ_{18b} (B_{2u})	1043		
υ_{18a} (B_{3u})	1074	1065	
υ_{9a} (B_{3u})	1222	1220	1230
Ω			1295
$\upsilon_{3-9b-15}$ (B_{2u})	1323		1345 (?)
υ_{19b} (B_{2u})	1411	1402*	
υ_{19a} (B_{3u})	1490	1484	
υ_{8b} (B_{2u})	1532	1527*	
υ_{8a} (B_{3u})	1598	1601	

B. Raman and in Situ SERS Experiments

mode (symmetry)	Raman υ/cm^{-1} bulk crystal	SERS (0.20 V) υ/cm^{-1} Au(poly)/OxRed
A_g	1001	1017
A_g (?)	1076	1072
A_g	1231	1222
A_g	1302	1289
B_{1g}	1324	
B_{1g}	1428	
A_g	1514	1504
A_g	1606 (1615)	1607

[a] The SEIRAS modes marked by "asterisks" were found in regions II, III, and IV. The SFG experiments have been limited to the range 1150 cm^{-1} < υ < 1450 cm^{-1}. Characteristic individual spectra are plotted in Figure 7 and Figure 8.

(62) Barker, D. J.; Buchleton, J. S.; Clark, G. R.; Cooney, R. P.; Richard, C. E. F. *J. Mol. Struct.* **1990**, *239*, 249.
(63) Metiu, H. *Prog. Surf. Sci.* **1984**, *17*, 153.
(64) Brolo, A.; Irish, D. E. *J. Electroanal. Chem.* **1996**, *414*, 188.

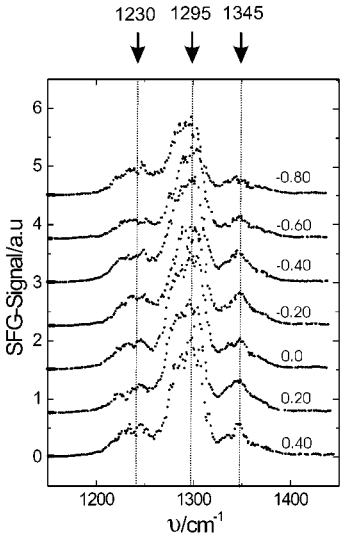

Figure 8. Selected potential-dependent SFG spectra of 3 mM 4,4′-BP in 0.05 M $KClO_4$ on Au(111).[49]

(ν_{12}) all SERS-active Ag vibrations exhibit counterparts of B_{3u} symmetry at rather similar wavenumbers in the SEIRA spectrum. This coincidence of SER and SEIRA spectra supports the symmetry reduction toward C_{2v} implying that all vibrational modes become Raman-allowed (cf. pyrazine in ref 58). Despite the fact that the inter-ring stretching mode $\Omega \sim 1289\ cm^{-1}$ is not found in the SEIRA spectrum, we can conclude from the existence of a distinct resonance feature around 1295 cm^{-1}, as reported in a recent visible-infrared in situ SFG experiment[49] (Figure 8), that this mode is indeed IR active for adsorbed 4,4′-BP on Au(111) in region I. Other SFG-active resonances in the range $1150\ cm^{-1} < \upsilon < 1450\ cm^{-1}$ were found around 1230 cm^{-1} (υ_{9a}) and 1345 cm^{-1}. The intensity decreases with more negative potential while the peak position remains rather constant. The nature of υ_{1345} is not yet clear.[49] We recall that the detection of a SFG resonance requires as a necessary condition its simultaneous IR **and** Raman activity.[3]

4.2. Orientation of 4,4′-BP in Regions II, II, and IV. (1) The increasing loss intensity of all SEIRAS-active B_{3u} modes (Figures 5 and 6), (2) the simultaneous occurrence of two new in-plane B_{2u} vibrations, ν_{1405} (ν_{19b}) (m), ν_{1527} (ν_{8b}) (w), with the latter having also a weak counterpart in the SER spectrum,[48] and (3) the absence of out-of-plane B_{2g} SERS modes at $\nu < 1000\ cm^{-1}$ demonstrate that the partial desorption of 4,4′-BP at E < P1 is accompanied by an in-plane tilt of the remaining surface-bound organic molecules in the *yz* plane. The N coordination between 4,4′-BP and the gold surface and the dominant lateral interactions between the adsorbed molecules (π stacking) seem to remain unchanged, as indicated by the potential dependence of the positions of the respective vibrational modes and of the baseline intensity. The exact tilt angle could not be determined. The potential dependence of the most prominent stretching band ν_{1601} (ν_{8a}) suggests two possible "tilt steps", which could be associated with the adlayers II and III. Both structures have been characterized in high-resolution in situ STM experiments[31] (Figure 9B,C). The decrease of the Raman intensity of the symmetrical A_g modes with more negative electrode potentials correlates with this interpetation (Figure 6A). In addition, one may conclude from the existence of these modes at potentials even more negative than −0.600 V (Figure 7D, Figure 8) that the reduction of 4,4′-BP past P3 occurs not in a completely flat but rather in slightly tilted orientation with reduction products remaining partially adsorbed on the surface.[32,33,48]

4.3. Comparison with Other N-Heterocyclic Molecules and Role of Coadsorbed Water. Macroscopic and molecular monolayer models[65,66] represent the adsorption of solute (A) and solvent molecules at metal/aqueous electrolyte interfaces by equations of the following type[67]

$$A_{bulk} + nH_2O_{ads} \leftrightarrow A_{ads}^{\ \lambda} + nH_2O_{bulk} + \lambda e^- \qquad (2)$$

λe^- represents the transfer of λ electrons.

Combined thermodynamic (chronocoulometry) and structure-sensitive studies with well-defined electrodes demonstrated that the adsorption of organic molecules is influenced by the properties of interfacial water ("hydrophobic effect"[68,69]), ions of the supporting electrolyte, structural properties of the solute (hydrogen bonding, π stacking, substrate−adsorbate coordination, ion pairing, ...), and the substrate surface (crystallographic orientation, material).[70,71] The adsorption of monofunctional aliphatic compounds on gold surfaces has the character of weak physisorption, which is dominated by Au−H_2O, A−H_2O, and H_2O−H_2O interactions (hydrophobic expulsion[68]) modified by the interfacial electric field.[72,66] On the other hand, adsorption between aromatic nitrogen-containing heterocyclic molecules and a gold electrode has the character of weak chemisorption (metal−ligand interaction), which involves predominantly either (1) interactions between the π electrons of the aromatic ring and the delocalized, polarizable free electrons in the metal or (2) a mixing of the N-lone pair orbitals with the electronic states of the metal.[70] Depending on the applied electrode potential, the heterocyclic adsorbate may assume both (1) a π-bonded or flat-lying position with the aromatic ring parallel to the negatively charged surface and (2) N-bonded (vertical, tilted, and/or rotated) orientations. In the following we will discuss our results of 4,4′-BP in comparison to the interfacial properties of other N-heterocyclic molecules adsorbed on massive or thin, quasi-single crystalline gold electrodes.

Flat orientations, in which the aromatic rings of the molecule are oriented parallel to the electrode surface, was reported for pyridine (Py),[73,56] pyrazine (pz),[74,75] and 2,2′-bipyridine (2,2′-BP)[76,77,78] based on chronocoulometry, in situ STM, and ex situ XPS studies. In situ SEIRAS

(65) Damaskin, B. B.; Petrii, O. A.; Batrakov, V. V. *Adsorption organischer Verbindungen an Elektroden*; Akademie-Verlag: Berlin, 1975.
(66) Cf. reviews in: *Adsorption of Molecules at Metal Electrodes*; Lipkowski, J., Ross, P. N., Eds.; VCH: New York, 1992.
(67) Koppitz, F. D.; Schultze, J. W.; Rolle, R. D. *J. Electroanal. Chem.* **1984**, *170*, 5.
(68) Israelachvili, J. *Intermolecular and Surface Forces*; Academic Press: London, 1992.
(69) Tabor, D. *J. Colloid Interface Sci.* **1977**, *58*, 2.
(70) Lipkowski, J.; Stolberg, L.; Yang, D. F.; Pettinger, B.; Mirwald, S.; Henglein, F.; Kolb, D. M. *Electrochim. Acta* **1994**, *39*, 1045.
(71) *Interfacial Electrochemistry*; Wieckowski, A., Ed.; M. Dekker, Inc.: New York, 1999.
(72) Beltowska-Brzezinska, M.; Luszak, T.; Holze, R. *Surf. Sci.* **1998**, *418*, 281.
(73) Stolberg, L.; Morin, S.; Lipkowski, J.; Irish, D. E. *J. Electroanal. Chem.* **1991**, *307*, 241.
(74) Ianelli, A.; Merza, J.; Lipkowski, J. *J. Electroanal. Chem.* **1994**, *376*, 49.
(75) Hamm, U.; Lazarescu, V.; Kolb, D. M. *J. Chem. Soc., Faraday Trans.* **1996**, *92*, 3785.
(76) Yang, D. F.; Bizzotto, D.; Lipkowski, J.; Pettinger, B.; Mirwald, S. *J. Phys. Chem.* **1994**, *98*, 7083.
(77) Cunha, F.; Tao, N. J. *Phys. Rev. Lett.* **1995**, *75*, 2376.
(78) Dretschkow, Th.; Lampner, D.; Wandlowski, Th. *J. Electroanal. Chem.* **1998**, *458*, 121.

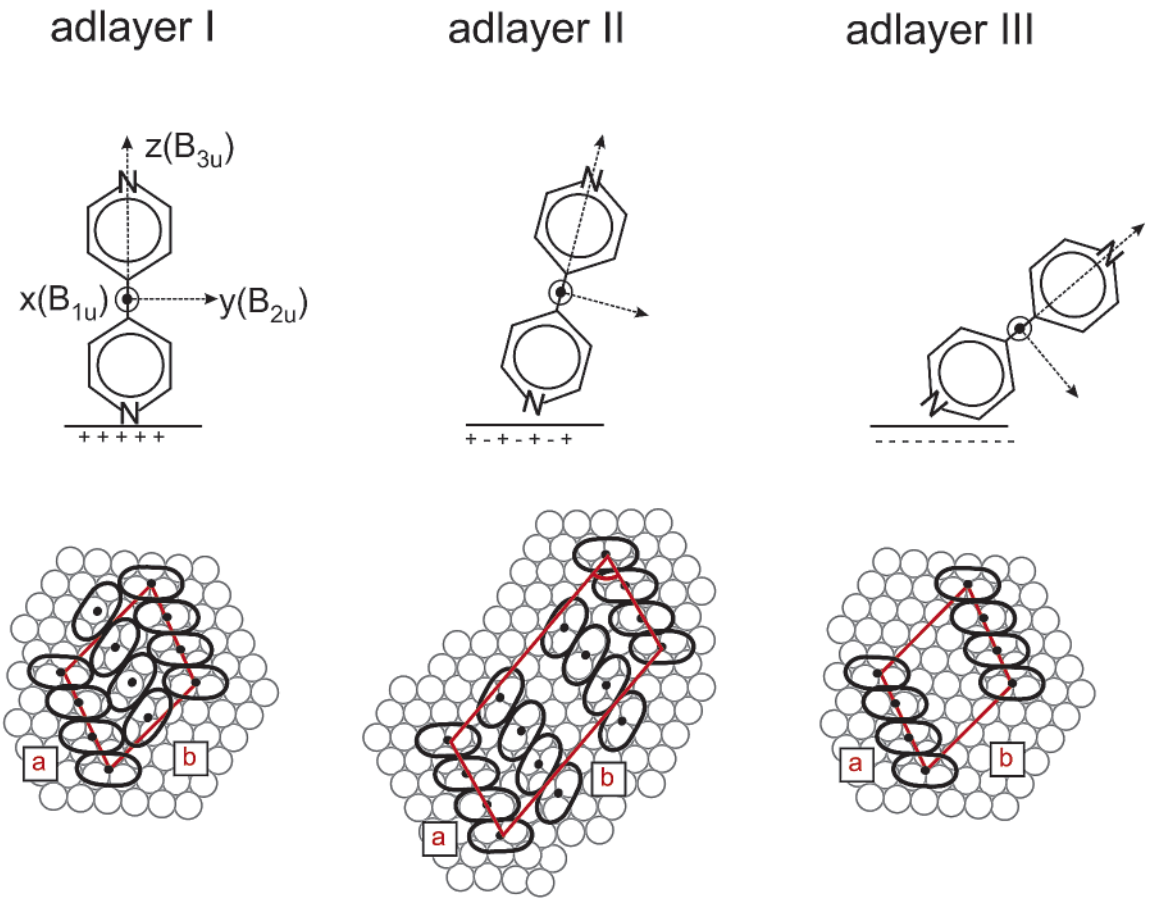

Figure 9. Orientation (derived from SEIRAS experiments) and packing (STM[31]) models of 4,4′-BP on Au(111).

experiments,[56,58,79] which only probe the Helmholtz and Gouy regions, revealed that the formation of the π-bonded adsorption state of all three molecules is accompanied by the replacement of water molecules from the electrode surface, in accord with the model expressed by eq 2. Detailed analysis of the bending mode of water, δ_{HOH}, as reported for pyridine,[56] showed that the loss features consists of two components representing individual and hydrogen-bonded water molecules. Upon changing the electrode potential, all three heterocyclic molecules coordinate to the positively charged surface with one (Py, Pz) or, in a coplanar cis-configuration, with both nitrogen atoms (2,2′-BP). This type of adsorbate−substrate coordination reduces the molecular symmetry to C_{2v}, and as a consequence all vibrational modes become Raman active.[58,79] Comparable SERS, IRAS, SEIRAS, and SFG investigations showed that the high coverage phase of Py represents a slightly rotated and end-on configuration,[56,61,80] while Pz and 2,2′-BP are both vertically oriented.[58,79,81] These coordinated adsorption states are stabilized by attractive, lateral π-stacking interactions between adjacent aromatic rings giving rise to two-dimensional ordered monolayers. Typical contrast pattern of in situ STM experiments revealed large domains of parallel molecular stacking rows separated by 0.9−1.5 nm with intermolecular distances of 0.38−0.45 nm and molecules tilted up to 30° from the normal of the chain axis.[56,77,78,82] Py and 2,2′-BP form the same stacking pattern in neutral and in acidic solutions, e.g., under conditions where at least one nitrogen atom is protonated in the bulk phase.[56,77−79] This result reflects the strength of the chemisorbed adlayer. Similar close-packed N-coordinated 2D stacking structures were also reported for 1,10′-phenanthroline (Phen)[83] and 2,2′-6,2″-terpyridine (TP)[84] on Au(111). All five molecules are coordinated to the metal surface through the nitrogen heteroatom and with the phenyl ring(s) directed toward the bulk electrolyte, which causes the hydrophobic hydration[68,85] of the organic adlayer, accompanied with the displacement of surface water according to eq 2. This, mainly entropic phenomenon arises from the structural rearrangement of water molecules in the overlapping solvation zones as two (or more) organic adspecies approach each other.[68] SEIRA spectra of Py, Pz, and 2,2′-BP indeed show pronounced water loss features in the OH bending (δ_{HOH}) and the OH stretching (ν_{OH}) regions with increasing adsorbate coverage.[56,58,79] One also notices that the N-bonded adsorption causes (1) a shift of the prominent symmetric A_1 molecular ring modes (in C_{2v} symmetry) toward higher wavenumbers, compared to the corresponding vibrations of the free molecule, and (2) an increase in the baseline level of the spectra. The latter represents the background reflectivity of the electrode or, in other words, the optical properties of the metal.[86,87] Both trends are more pronounced with

(79) Noda, H.; Minoha, T.; Wan, L. J.; Osawa, M. *J. Electroanal. Chem*. **2000**, *481*, 62.
(80) Hebert, P.; Le Rille, A.; Zheng, W. Q.; Tadjeddine, A. *J. Electroanal. Chem*. **1998**, *447*, 5.
(81) Hoon-Khosla, M.; Fawcett, W. R.; Goddard, J. D.; Tian, W. Q.; Lipkowski, J. *Langmuir* **2000**, *16*, 2356.
(82) Andreasen, G.; Vela, M. E.; Salvarezza, R. C.; Arvia, A. J. *Langmuir* **1997**, *13*, 6814.
(83) Cunha, F.; Jin, Q.; Tao, N. J.; Li, C. Z. *Surf. Sci*. **1997**, *389*, 19.
(84) Pinheiro, L. S.; Temperini, M. L. A. *Surf. Sci*. **2000**, *464*, 176.
(85) Conway, B. E.; Mathieson, J. G.; Dhar, H. P. *J. Phys. Chem*. **1974**, *78*, 1226.
(86) Ataka, K.; Osawa, M. *J. Electroanal. Chem*. **1999**, *460*, 188.

increasing strength of chemisorption of the adsorbate (Pz < Py < 2,2′-BP[56,58,79]).

The adsorption of 4,4′-BP on Au(111) reveals some subtle differences, in comparison to Py, Pz, 2,2′-BP, Phen, and TP: The formation of the anion radical prevented an unambiguous conclusion on a possible flat orientation of 4,4′-BP at sufficiently negative potentials in the low coverage region.[31,38] At $E > -0.500$, e.g., still at a negatively charged electrode, a first in-plane tilted N-coordinated adlayer is formed, which transforms into a densely packed, interdigitated stacking pattern of all-perpendicularly arranged 4,4′-BP molecules at a positively charged Au(111) surface in two discrete steps[31] (Figure 9). The surface coordination is rather weak, as indicated by (1) the small upshift of the A_1 ring frequencies in C_{2v} geometry and (2) the potential independence of the baseline level (Table 1). The absolute SEIRA spectra reveal (cf. Figure 3) that the increase of the 4,4′-BP coverage is accompanied by an increase of oriented interfacial water, as compared with the adsorbate-free reference. The narrower bandwidth, ~214 cm^{-1}, of the OH stretching contribution for strong hydrogen bonding, υ_{OH} (3484 cm^{-1}), and of the bending mode, δ_{HOH} at 1650 cm^{-1} with 87 cm^{-1} (fwhm), compared to bulk water (400 cm^{-1} at 3370 cm^{-1} and 100 cm^{-1} at 1648 cm^{-1}) suggest an ordered water structure surrounding the 4,4′-BP monolayer. The second nitrogen, which faces the electrolyte, can directly participate in hydrogen bonding to the adjacent solvent molecules. This configuration is valid in all three potential regions of N-coordinated 4,4′-BP. The hydrophilic adsorption, e.g., the co-deposition of densely packed 4,4′-BP and (at least) second-layer ordered water molecules is supported by (1) EQCM experiments, where Wilde et al. could not find any mass changes upon 4,4′-BP adsorption on gold film electrodes[35] as well as (2) by the high sensitivity of the STM contrast pattern of 4,4′-BP in the N-coordinated phases to tunneling currents larger than 30 pA. (Steady-state imaging requires unusually large distances between sample and tip!)[31] The classical picture, "substitution of solvent molecules by adsorbed organic species", as represented by eq 2 is not valid. Remarkable structural changes of the electrolyte may occur within the entire interfacial region of density inhomogeneities (usually only two, at most three layers[88]) that parallel the formation of hydrophilic organic monolayers. The unique sensitivity and selectivity, and its exclusive penetration depth into the Helmholtz and Gouy regions,[5] qualify SEIRAS as an ideal approach to explore these phenomena in detail. Futamata et al.[37] reported, for instance, in an ATR-IR study that diprotonated 4,4′-BPH_2^{2+} adsorbs only in perchlorate containing electrolyte in direct contact with the gold surface, while more strongly adsorbed SO_4^{2-} or Cl^- ions expel 4,4′-BPH_2^{2+} into the second layer outside the contact-adsorbed anions. The adsorbate-induced co-formation of ordered water in the electrochemical double layer region of Au(111)/electrolyte interfaces was also observed for Cu underpotential deposition (UPD) in H_2SO_4[87] (but not for Pb UPD neither in H_2SO_4 nor in $HClO_4$ due to the complete discharge of the Pb^{2+}!), the deposition of fumaric acid,[89] and 4-mercaptopyridine.[90] The common features of all these systems are hydrophilic groups (SO_4^{2-}, $-COO^-$, $\rangle N|$) exposed to the electrolyte. We speculate (due to the current lack of experimental data) that many organic spacers with functional groups that act as "bait" to promote surface binding and operation of proteins like cytochrome *c*, such as carboxylates, sulfonates, phosphates or 4-pyridyl, and aniline-type amines, $ArNH_2$,[21] undergo hydrophilic adsorption on gold surfaces and induce a high order of interfacial water. If the hydrophilic groups are blocked, for instance, by surface coordination as in the case of cytosine[86] or uracil[91] on Au(111), classical hydrophobic adsorption and phase formation are observed. SEIRAS appears to be a valuable tool to develop these structural concepts further.

Acknowledgment. The present work was supported by the Volkswagen Foundation (77/116), the EG through IC-014-00, and the Research Center Jülich. K.A. is indebted to the Alexander von Humboldt Foundation for a Research Fellowship. The authors also acknowledge the support of Professor Ibach, the stimulating discussions with Professor Z. Q. Tian, Professor A. Tadjeddine, and Dr. D. Diesing, and technical assistance of J. Ikonomov.

LA025585K

(87) Futamata, M. *Chem. Phys. Lett.* **2001**, *333*, 337.

(88) Spohr, E. *Habilitation*, University of Ulm, 1995.

(89) Noda, H.; Ataka, K.; Wan, L. J.; Osawa, M. *Surf. Sci.* **1999**, *427−428*, 190.

(90) Hara, Y.; Wan, L. J.; Noda, H.; Taniguchi, I.; Osawa, M. *J. Electroanal. Chem.*, in press.

(91) Pronkin, S.; Wandlowski, Th. In preparation.